Non-invasive longitudinal imaging of tumor progression using an ^{111}Indium labeled CXCR4 peptide antagonist

Tessa Buckle[1], Nynke S van den Berg[1], Joeri Kuil[1], Anton Bunschoten[1], Joppe Oldenburg[1], Alexander D Borowsky[2], Jelle Wesseling[3], Ryo Masada[4], Shinya Oishi[4], Nobutaka Fujii[4], Fijs WB van Leeuwen[1]

Supporting information

Methods:

Ac-TZ14011

Ac-TZ14011 was synthesized according to previously described procedures (see main manuscript).[1]

4F-Bz-TZ14011

Linear 4F-Bz-TZ14011 was synthesized following standard Fmoc/*t*Bu solid phase peptide chemistry on an amide resin (200 µmol scale). MS: $[M+3H]^{3+}$ calculated 730.37, found 730.43. The peptide was cyclized via a disulfide bond by stirring for 48 hours in 4% DMSO in water at a concentration of 0.4 mg/mL. After concentration *in vacuo* the product was purified by preparative HPLC using a Waters 1525EF HPLC system equipped with a 2489 UV detector operating at 220 nm and a Dr. Maisch Reprosil-pur C18-AQ 10 µm (250 × 20 mm) column. A gradient of 0.1% TFA in H_2O/CH_3CN 95:5 to 0.1% TFA in H_2O/CH_3CN 5:95 in 40 minutes was used. The product was obtained as a white fluffy solid after pooling of the appropriate fractions and lyophilization. MS: $[M+3H]^{3+}$ calculated 729.69, found 729.42.

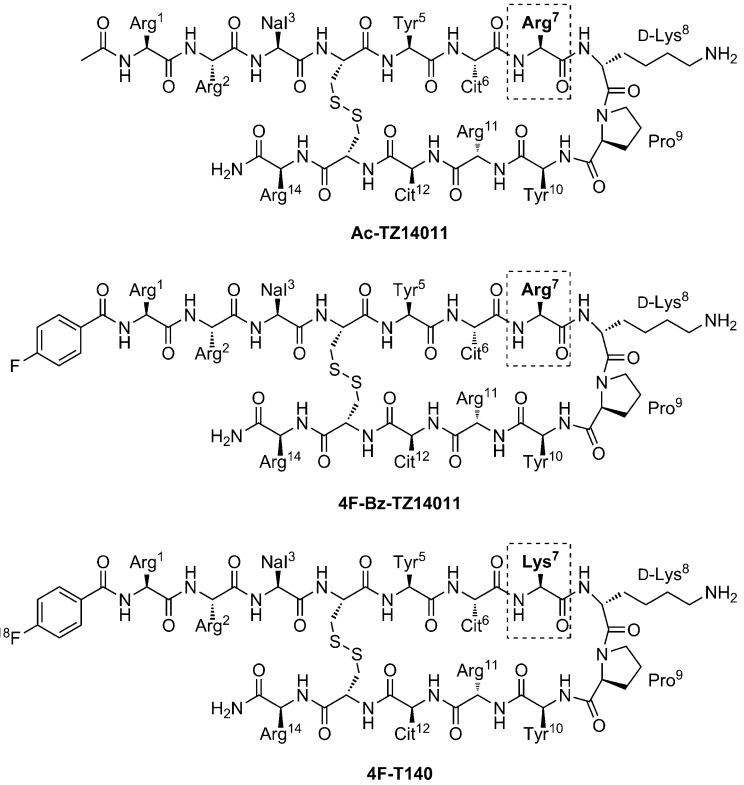

Figure S1. Structures of the unlabeled peptides used in this study and the 4F-T140 peptide, which was used in a recent study [2]. Amino acid residue 7 differs in T140 compared to TZ14011 as indicated by the dotted rectangle.

DTPA-Ac-TZ14011

DTPA-Ac-TZ14011 was synthesized according to previously described procedures (see main manuscript) [1].

DTPA-4F-Bz-TZ14011

DTPA(tBu)$_4$ (1.85 mg, 3.0 µmol) was preactivated by addition of PyBOP (1.56 mg, 3.0 µmol), HOBt (0.4 mg, 3.0 µmol) and DiPEA (4.1 µL, 25 µmol) in DMF (2 mL). After 5 minutes of stirring, 4F-Bz-TZ14011 (7.2 mg, 2.5 µmol) was added and the reaction was stirred overnight. After concentration *in vacuo*, the *t*-butyl groups were removed by stirring in 95% TFA/2.5% TIS/2.5% water (5 mL) for two hours. The product was precipitated in cold MTBE/hexane, dissolved in water/CH_3CN (2 mL) and lyophilized. The product was purified by preperative HPLC as described above for 4F-Bz-TZ14011. DTPA-4F-Bz-TZ14011 was obtained as a white fluffy solid (3.7 mg, 47 %) after pooling of the appropriate fractions and lyophilization. MS: $[M+3H]^{3+}$ calculated 854.74, found 854.52.
Radiolabeling with ^{111}In and biodistribution studies were carried out as stated in the material and methods of the main manuscript.

MSAP-Ac-TZ14011
MSAP-Ac-TZ14011 was synthesized according to previously described procedures [3].

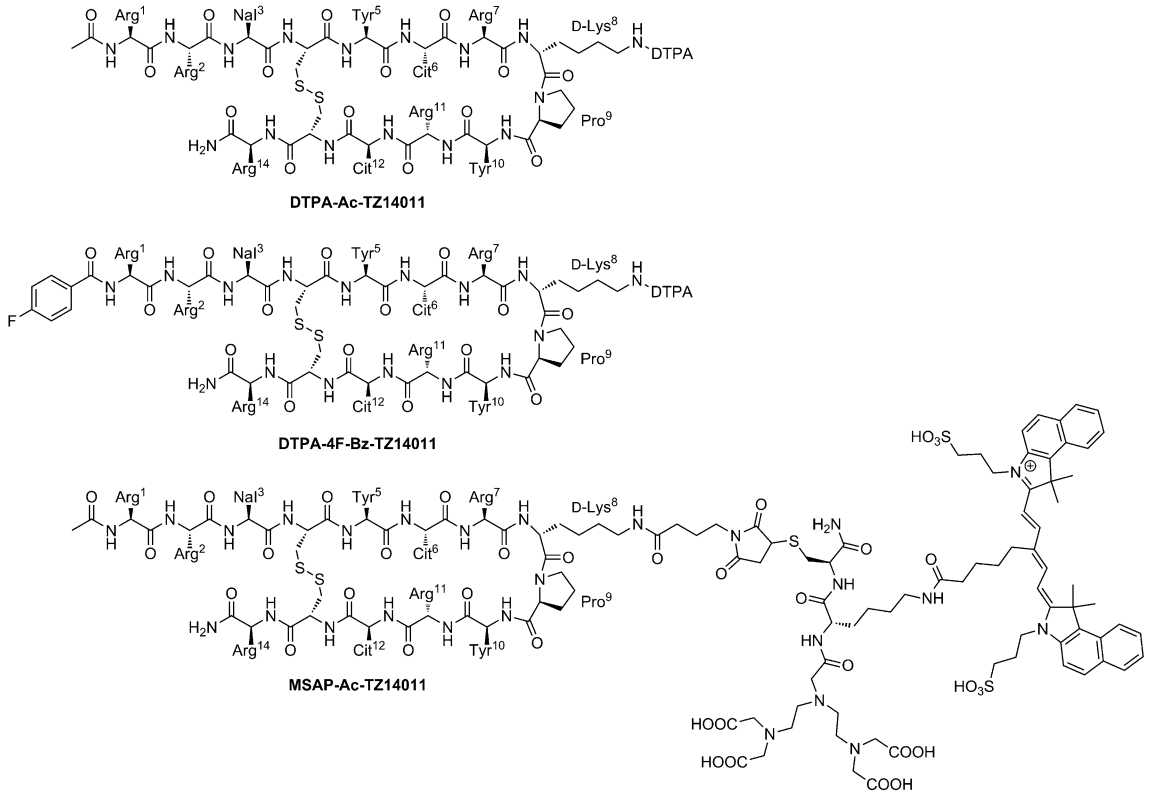

Figure S2. Structures of the labeled peptides used in this study.

Synthesis and radiolabeling DTPA-c[RGDfK]

The RGD peptide, c[RGDfK], binds to the $\alpha_3\beta_5$ integrin receptor, of which expression has been linked to angiogenesis [4]. c[RGDfK] was synthesized by Fmoc/*t*Bu-SPPS on a trityl resin. The protected peptide was cleaved from the resin and cyclized head-to-tail with BOP/HOBt. After purification by silica column chromatography, the remaining protecting groups were removed and the product was purified by RP-HPLC.

DTPA-c[RGDfK] was synthesized by reacting the *in situ* formed succinimidyl ester of DTPA(tBu)$_4$ with c[RGDfK]. The protecting groups were removed with TFA/TIS/water and the product was purified by RP-HPLC. For imaging of 1 mouse, 25 μg of DTPA-c[RGDfK] was dissolved in 50 μL 0.1M acetic acid and 25 μl InCl3 (10 MBq) was added. After 30 minutes of incubation, labeling was validated using thin layer chromatography. In all cases, labeling efficacy was >99%. Before injection, 100 μL of saline was added.

Determination of K_D values

MDAMB231^{CXCR4+} cells were cultured under standard conditions in MEM medium containing MEM vitamins, L-glutamin, non-essential amino acids, natrium/pyruvate and penicillin/streptomycin solution (all BD Biosciences). Cells were trypsinized and aliquoted in portions of 300,000 cells, centrifuged (1200 rpm, 5 min, 4 °C) and decanted. Different concentrations (0–10000nM) of DTPA-Ac-TZ14011 or DTPA-4F-Bz-TZ14011 in the presence of 250nM of MSAP-Ac-TZ14011 in 50 µL of 0.1% bovine serum albumin (BSA) in phosphate buffered saline (PBS) were added. Cells were incubated for 1 hour at 4 °C. The cells were washed with 300 µL of 0.1% BSA in PBS, resuspended in 300 µL of 0.1% BSA in PBS and fluorescence was measured using a CyAn ADP flow cytometer (DakoCytomation) with APC-Cy7 settings (635 nm laser and 750nm long pass filter). Live cells were gated on forward scatter, side scatter and pulse width and 20,000 viable cells were analyzed. All experiments were performed in duplicate.

The normalized geometric means were fitted with equations in the GraphPad Prism 5 software. The K_D values of DTPA-Ac-TZ14011 and DTPA-4F-Bz-TZ14011 were calculated using the 'Binding – Competitive, One site – Fit logK_i' nonlinear regression equation (Eq. 1 and 2). The K_D value of MSAP-Ac-TZ14011 (186.9 nM) has previously been reported [3]. K_D values were determined in the absence of indium as previously was shown that indium binding to MSAP-Ac-TZ14011 does not affect the interaction with CXCR4, because the label is distance from the pharmacophore [3]. This is in contrast to a cyclic pentapeptide reported by Demmer *et al*., where the DOTA label is in close proximity to the binding site, resulting in a significant change in CXCR4 binding affinity upon indium binding of the DOTA peptide [5].

$$\log IC_{50} = \log\left(10^{\log K_D} * \left(1 + \frac{[MSAP-Ac-TZ14011]}{K_{D,\,MSAP-Ac-TZ14011}}\right)\right) \quad \text{(Eq. 1)}$$

$$y = Bottom + \frac{Top - Bottom}{1 + 10^{(x - \log IC_{50})}} \quad \text{(Eq. 2)}$$

IC_{50} = concentration of competitor that results in binding half-way between Bottom and Top
K_D = equilibrium dissociation constant of the competitor in nM
[Ac-TZ14011-MSAP] = concentration of MSAP-Ac-TZ14011 (250 nM)
$K_{D,\,MSAP\text{-}Ac\text{-}TZ14011}$ = dissociation constant of MSAP-Ac-TZ14011 (186.9 nM)
y = normalized fluorescence
Bottom and Top = plateaus in the units of the y axis
x = concentration of the competitor in nM

Results and Discussion:

Optimization of the CXCR4-targeting peptide might further increase the specific tumor uptake and improve the distribution. For example, Jacobsen *et al.* recently showed that liver uptake, using a derivative of T140 that only differs slightly from Ac-TZ14011, is significantly decreased and should therefore be a better peptide candidate [2]. We used 4F-Bz-14011, a peptide similar to that used by Jacobsen *et al.* as a reference for Ac-TZ14011.

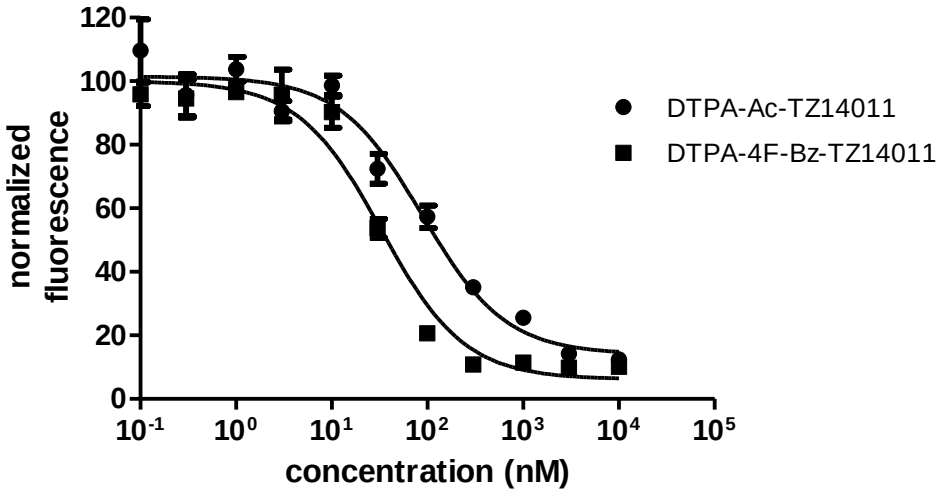

Figure S3. Competition experiments with DTPA-Ac-TZ14011 and DTPA-4F-Bz-TZ14011 peptides in the presence of 250 nM of MSAP-Ac-TZ14011.

Table S1. Dissociations constants (K_D) of the constructs.

Construct	**K_D (nM)**
DTPA-Ac-TZ14011	37.89 ± 7.87
DTPA-4F-Bz-TZ14011	14.13 ± 2.67

In flow cytometric experiments wherein the affinity for the CXCR4 receptor of these peptides was measured, DTPA-4F-Bz-14011 showed a 2-fold lower K_D compared to DTPA-Ac-TZ14011 (**Figure S3**, **Table S1**). Attachment of a DTPA chelate has a negative influence on the binding affinity of Ac-TZ-14011 [3]. Unfortunately, this is a necessary evil in CXCR4 imaging using T140 based peptides. A comparison between DTPA-4F-Bz-14011 and DTPA-Ac-TZ14011 revealed that the differences in affinity for the CXCR4 receptor for the different peptide moieties did not result in differences in distribution or in better results *in vivo* as tumor-to-muscle ratio's were comparable (**Table 3** and **Table S2**).

It has been reported that by replacing the acetyl (Ac) group at the N-terminus for a 4-fluorobenzoyl (4-F-BZ) the anti-HIV activity increased by approximately a factor 7 (See Tamamura *et al.*; compound TF14015 and TF14016 [6]). However in this article, Ac-TZ14011 analogs were used in stead of Ac-TZ14011. These peptides only differ at amino acid position 7 (Ac-TZ14011; Arg^7; TF14015 and TF14016: Lys^7). Since this amino acid is not important for CXCR4 receptor binding [7], we did not expect large differences. More importantly, to fairly evaluate the effect of the 4-F-BZ group we only replaced Ac for 4-F-BZ whereas the rest of the peptide was identical.

Table S2: Distribution of ^{111}In-DTPA-4F-Bz-14011

	%ID/g
Blood	0.06 ± 0.03
Brain	0.01 ± 0.00
Lungs	0.41 ± 0.02
Heart	0.16 ± 0.04
Liver	7.35 ± 0.42
Kidneys	28.71 ± 0.92
Spleen	2.68 ± 0.39
Stomach	0.14 ± 0.02

Intestines	0.27 ± 0.00
Muscle (paw)	0.06 ± 0.02
Axilary LN	3.35 ± 0.74

In the MIN-O tumor model, uptake levels of ^{111}In-DTPA-Ac-TZ14011 increase with progression of lesion size, which is identical to results shown with ^{18}F-FDG PET [9]. However, accumulation of the metabolic tracer ^{18}F-FDG in the 4T1 control tumors has also been reported [8]. Clearly, the uptake of targeted imaging agents in the tumor needs to be directly related to the level of receptor expression in the tumor cells and therefore influence of additional factors need to be excluded. One of these factors is perfusion. Increase in the amount of new blood vessels can increase perfusion of a tumor lesion resulting in higher uptake of an imaging agent, which could obscure the interpretation of the imaging data. Evidence that the uptake of ^{111}In-DTPA-Ac-TZ14011 is not governed by the degree of tumor angiogenesis is provided by the SPECT/CT experiments, as data obtained with ^{111}In-DTPA-c[RGDfK] shows a comparable uptake in both tumor types. **Figure S2** shows that in both 4T1 and MIN-O lesions, uptake of ^{111}In-c[RGDfK]-DTPA increased with increasing lesion size and that for this tracer no significant difference between the progressive uptake in the MIN-O and 4T1 tumor lesions was observed.

Unlike SPECT/CT imaging with ^{111}In-DTPA-Ac-TZ14011, lesions were only followed until they reached 400 mm^3. Especially in larger 4T1 lesions, necrosis in the tumor core had a negative effect on the uptake of ^{111}In-c[RGDfK]-DTPA. In these tumors, unreliable uptake values were measured which were probably caused by non-specific uptake in the necrotic core.

This, combined with the absence of membranous staining in the control tumors and the increase in membranous staining in intermediate and late stage MIN-O tumor lesions seen with IHC and flow cytometry (See **Figure 2** and **Tables 1&2**),underlines that the uptake of the ^{111}In-DTPA-Ac-TZ14011 in the MIN-O lesions is driven by the presence of the CXCR4 receptor on the membrane of the cell.

References

[1] Hanaoka H, Mukai T, Tamamura H, Mori T, Ishino S, Ogawa K, Iida Y, Doi R, Fujii N, and Saji H. Development of a ^{111}In-labeled peptide derivative targeting a chemokine receptor, CXCR4, for imaging tumors. Nucl Med Biol 2006,*33*:489-494.

[2] Jacobson O, Weiss ID, Kiesewetter DO, Farber JM, Chen X. PET of tumor CXCR4 expression with 4-^{18}F-T140. J Nucl Med 2010;51:1796-1804.

[3] Kuil J, Buckle T, Yuan H, van den Berg NS, Oishi S, Fujii N, Josephson L, van Leeuwen FWB. Synthesis and evaluation of a bimodal CXCR4 antagonistic peptide**.** Bioconjugate Chem. 2011;22(5):859-864

[4] Beer AJ, Schwaiger M. Imaging of integrin $\alpha_3\beta_5$ expression. Cancer Metastasis Rev. 2008; 27: 631-644

[5] Demmer O, Gourni E, Schumacher U, Kessler H, Wester HJ, PET imaging of CXCR4 receptors in cancer by a new optimized ligand. Chem Med Chem, 2011;6,1789-1791.

[6] Tamamura H, Hiramatsu K, Mizumoto M, Ueda S, Kusano S, Terakubo S, Akamatsu M, Yamamoto N, Trent J, Wang Z, Peiper S, Nakashima H, Otaka A, Fujii N. Enhancement of the T140-based pharmacophores leads to the development of more potent and bio-stable CXCR4 antagonists. Org Biomol Chem. 2003;1:3663-3669

[7] Trent JO, Wang Z, Murray JL, Shao W, Tamamura H, Fujii N, Peiper SC. Lipid bilayer simulations of CXCR4 with inverse agonists and weak partial agonists. J Biol Chem. 2003;278(47);47136-47144

[8] Cao Q, Cai W, Niu G, He L, Chen X. Multimodality imaging of IL-18-binding protein-Fc therapy of experimental lung metastasis. Clin Cancer Res. 2008;14(19): 6137-6145

[9] Abbey CK, Borowski AD, McGoldrick, Gregg JP, Maglione JE, Cardiff RD, Cherry SR. In vivo positron-emission tomography imaging of progression and transformation in a mouse model of mammary neoplasia. PNAS.